ACS OMEGA

http://pubs.acs.org/journal/acsodf

Article

Synthesis of Double-Walled Boron Nitride Nanotubes from Ammonia Borane by Thermal Plasma Methods

Dongsu Bae, Unseok Jung, Hunsu Lee, Heeil Yoo, Se Youn Moon, Kun-Hong Lee,* and Myung Jong Kim*

Cite This: *ACS Omega* 2023, 8, 21514−21521

Read Online

ACCESS | Metrics & More | Article Recommendations | Supporting Information

ABSTRACT: Highly crystalline double-walled boron nitride nanotubes (DWBNNTs ∼60%) were synthesized from ammonia borane (AB; $H_3B{-}NH_3$) precursors using a high-temperature thermal plasma method. The differences between the synthesized BNNTs using the hexagonal boron nitride (h-BN) precursor and AB precursor were compared using various techniques such as thermogravimetric analysis, X-ray diffraction, Fourier transform infrared spectroscopy, Raman spectroscopy, scanning electron microscopy, transmission electron microscopy, and in situ optical emission spectroscopy (OES). The synthesized BNNTs were longer and had fewer walls when the AB precursor was used than when the conventional method was used (with the h-BN precursor). The production rate significantly improved from ∼20 g/h (h-BN precursor) to ∼50 g/h (AB precursor), and the content of amorphous boron impurities was significantly reduced, implying a self-assembly mechanism of BN radicals rather than the conventional mechanism involving boron nanoballs. Through this mechanism, the BNNT growth, which was accompanied by an increased length, a decreased diameter, and a high growth rate, could be understood. The findings were also supported by in situ OES data. Considering the increased production yield, this synthesis method using AB precursors is expected to make an innovative contribution to the commercialization of BNNTs.

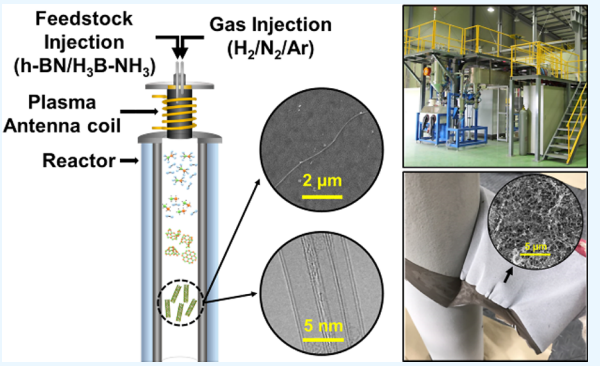

INTRODUCTION

Boron nitride nanotubes (BNNTs) are a type of one-dimensional nanomaterial structurally identical to carbon nanotubes (CNTs).[1] Here, boron and nitrogen atoms are alternatively bonded to each other and form hexagonal B−N lattices. BNNTs exhibit excellent intrinsic properties, such as mechanical properties,[2−4] thermo-mechanical stability,[5] high thermal conductivity,[6,7] and an oxidation resistance[8] similar to that of CNTs owing to their structural similarity. Owing to the difference in the electronegativities of boron and nitrogen,[9] BNNTs consist of polar covalent B−N bonds and are electrically insulating, with a band gap of ∼5−6 eV.[10,11] As half of the BNNT is composed of boron, which exhibits excellent neutron absorption, BNNTs have high neutron absorption capability[12] and are potential effective neutron-shielding materials in the aerospace industry.

The first BNNTs were synthesized by Chopra et al.[13] in 1995 by arc discharge and theoretically predicted by Rubio and co-workers.[10] Since then, various studies have been conducted to synthesize highly crystalline BNNTs using laser ablation,[14] ball milling,[15] and chemical vapor deposition (CVD).[16] The kinetic barrier in the synthesis of BNNTs is higher than that of CNTs because boron and nitrogen atoms must bond alternatively; therefore, the growth rate of BNNTs is considerably low. To overcome this kinetic barrier, several research groups have developed catalysts and used high temperatures. Boron oxide CVD (BOCVD) is one of the most promising methods for developing catalysts, wherein BNNTs are synthesized by the reaction between ammonia and B_2O_2 vapors, which are generated by the reaction of boron powder with metal oxides (e.g., MgO, FeO, and Li_2O).[17,18] However, the crystallinity, length, and number of walls of the BNNTs are not sufficient to industrially use the synthesized BNNTs. In recent years, studies have reported success with high-temperature methods to synthesize highly crystalline BNNTs by laser ablation[19] and thermal plasma.[20]

Smith et al.[19] reported a high-temperature pressure laser ablation method that can produce highly crystalline BNNTs by a reaction between spontaneously formed boron nanoballs (i.e., seeds) and ambient nitrogen gas. To use nitrogen gas as a reactant in the BNNT synthesis reaction, the triple bond of the

Received: January 24, 2023
Accepted: May 24, 2023
Published: June 7, 2023

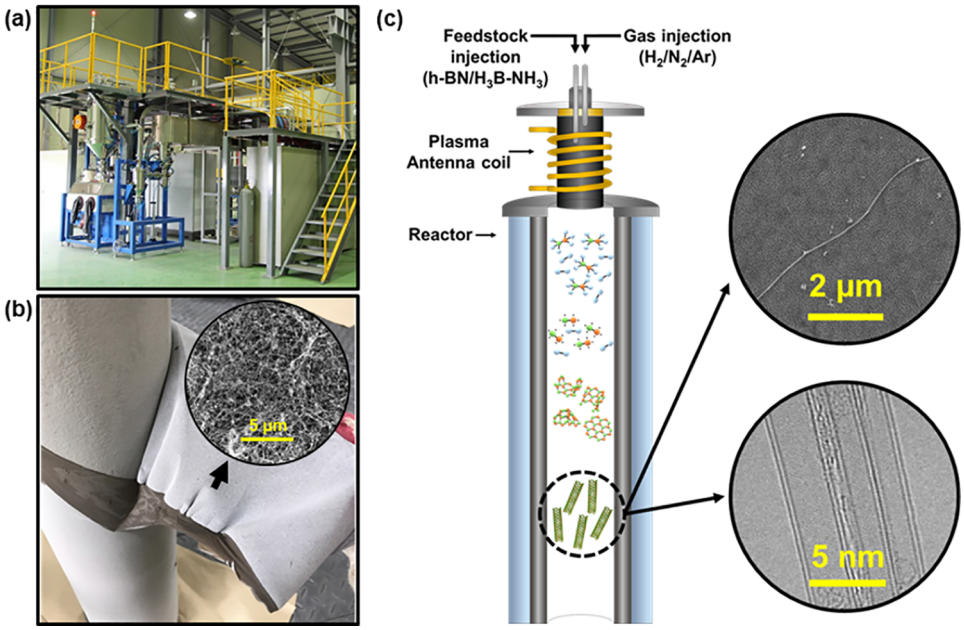

Figure 1. Photographs of the thermal plasma equipment. Overview of the (a) plasma system and (b) collected BNNTs in bucky paper form on the collecting rod; (c) schematic of the inside of the reactor and SEM/TEM images of the synthesized BNNTs.

nitrogen molecule (~10 eV binding energy) must be dissociated. Although the high kinetic barrier for nitrogen dissociation could be overcome by catalysts as in the Haber–Bosch process,[21] Smith et al. utilized the thermal energy of a continuous laser to overcome the kinetic barrier. Moreover, Kim et al.[22] suggested two growth mechanisms of BNNTs in high-temperature pressure laser ablation: a root growth mode from boron ball seeds and an open-end growth mode close to heterogeneous nucleation.

Kim et al.[20] grew BNNTs using h-BN as the precursor via the thermal plasma method at a high temperature of 8000 K. Boron and nitrogen were supplied by introducing h-BN, possessing a two-dimensional planar structure and consisting of B–N hexagons, into a high-temperature plasma reactor. The growth mechanism of BNNTs is considered to be initiated by boron nanoballs, similar to that in the laser ablation method by Smith et al.[19] B–N–H compounds are formed as intermediate species when hydrogen gas is also supplied with nitrogen and h-BN, the reaction initiates on the boron ball surface, and finally, the BNNT structure is formed. The two types of high-temperature BNNT synthesis methods, which currently provide the best results, are based on the use of boron nanoballs. In these methods, the formation of impurities such as amorphous boron is unavoidable. However, the presence of these impurities hinders efficient production and considerably interferes with the van der Waals interactions among the BNNTs, thus hindering the spontaneous formation of BNNT fibers.

Here, we propose the use of a molecular precursor, ammonia borane ($H_3B–NH_3$), which enables the independent supply of B–N radicals analogous to that from carbon atoms in CNT synthesis. $H_3B–NH_3$ comprises six hydrogen atoms bonded with B–N bonds. Because the bonding energies of the B–H (330 kJ/mol) and N–H (314 kJ/mol) bonds are lower than that of the B–N (389 kJ/mol) bond, on absorbing thermal energy, $H_3B–NH_3$ gradually decomposes, releases hydrogen gas, and converts to $–(B–N)_n–$, and then eventually forms a hexagonal BN structure.[23] Previous studies[24−26] have attempted to synthesize BNNTs using $H_3B–NH_3$ as a precursor; catalysts or templates were used to synthesize BNNTs at 1450–1700 °C but produced defective BNNTs with radii of several hundred nanometers. Therefore, the synthesis of few-walled and sufficiently long BNNTs for high-end applications has not been achieved thus far. The unsuccessful synthesis can be attributed to the fusion of BN network (–B–N–) domains, which are formed during the dehydrogenation of $H_3B–NH_3$ and generate multiple defects in the domains before BNNT formation.

To overcome this challenge, our group employed a laser ablation method[27] in which a high-power laser was used to instantaneously supply high energy to $H_3B–NH_3$. Compared to the conventional laser ablation method[19] which uses solid boron and nitrogen gas as precursors, the content of amorphous boron impurities was significantly reduced in this method, resulting in the spontaneous formation of BNNT fibers exceeding 10 cm in length. This method can provide B–N radicals from $H_3B–NH_3$, similar to the role of C_xH_y in CNT synthesis.

As mentioned earlier, even in the high-temperature thermal plasma method, the growth of BNNTs is initiated by boron nanoballs;[20] hence, the generation of amorphous boron impurities is inevitable. In addition, the growth rate is limited because the supply of boron and nitrogen is limited to the boron nanoball surface, which hinders the synthesis of long and few-walled BNNTs.

Herein, we report the synthesis of highly crystalline, long, and double-walled BNNTs (~60%) with minimal amorphous boron impurities through a thermal plasma method using $H_3B–NH_3$ as the precursor. BNNTs synthesized from h-BN and $H_3B–NH_3$ were compared and analyzed by various methods such as thermogravimetric analysis (TGA), X-ray diffraction (XRD), Fourier-transform infrared (FT-IR) spectroscopy, Raman spectroscopy, scanning electron microscopy (SEM), transmission electron microscopy (TEM), and in situ optical emission spectroscopy (OES). Using the $H_3B–NH_3$ precursor, the content of amorphous boron impurities

https://doi.org/10.1021/acsomega.3c00498
ACS Omega 2023, 8, 21514−21521

significantly decreased from 8.88 wt % (with h-BN) to 3.16 wt % (with H_3B-NH_3), and the boron nanoballs frequently observed at the end of BNNTs from the h-BN precursor (Figure S11) were no longer observed. This might indicate that the BNNT growth was not initiated by conventional boron nanoballs, but it can be interpreted as the self-assembly of BN radicals (Figure 1c), which increased the growth rate. The BNNTs were collected in a bucky paper form (Figures 1b and S10) and the production rate of BNNTs increased to 50 g/h (Figure S9) when H_3B-NH_3 was used as a precursor, compared to 20 g/h when h-BN was used.[20] Additionally, the average length of the BNNTs increased 2.27 times and average number of walls decreased from 3.24 (with h-BN) to 2.44 (with H_3B-NH_3).

EXPERIMENTAL METHODS

Synthesis of BNNTs. As shown in Figure 1c, two injection systems are installed at the reactor inlet. h-BN or H_3B-NH_3 precursors were supplied by feedstock injection in the powder form at a constant rate. The h-BN had a size of 70 nm, and H_3B-NH_3 (30.88 g/mol) was a white powder with a purity of 97% (Boron Specialties, LLC). Hydrogen/nitrogen gas was continuously supplied via gas injection at a constant rate. As the chemicals passed through the 60 kW radio frequency (RF) plasma reactor (PLASNIX Inc), the precursor was decomposed by the high energy, and the reactants produced from the RF plasma zone descended vertically down the reactor owing to gravity and the gas flow. The detailed plasma operating conditions are tabulated in Table 1. For both cases, hBN and H3B−NH3 (Ammonia Borane, AB), the plasma operation conditions were same to find the effect of feedstock. Finally, the BNNTs were synthesized; the entire process is shown as a schematic in Figure 1c. The synthesized BNNTs were collected in the collector and were first obtained in the form of bucky paper (Figure 1b).

Table 1. Process Conditions of the Synthesis of BNNTs

power	30−32 kW
frequency	2−4 MHz
pressure	680 torr
central gas (Ar)	30 slpm
sheath-axial gas (Ar)	10 slpm
sheath-tangential gas (Ar)	15 slpm
sheath gas (N_2)	60 slpm
sheath gas (H_2)	33 slpm
carrier gas (Ar)	15 slpm
feeding rate (AB)	0.4−2.2 g/min
feeding rate (h-BN)	0.4−1.0 g/min

In Situ OES. The light emission from the thermal plasma during the BNNT synthesis with h-BN and H_3B-NH_3 precursor is measured using in situ optical emission spectroscopy (OES; QE Pro, Ocean optics, USA). The OES is equipped with a HC-1 grating and 10 μm silt width, giving wavelength range from 248 to 1034 nm. The OES is measured from port 1 to port 5, and the distance between each port is 90 mm. In order to measure low light emission intensity, considering the light intensity decrease as the port number increases, the exposure times are set to be 10 s for port 1 and 2, 20 s for port 3 and 4, and 40 s for port 5, respectively and 25 times of measurements from each port is accumulated to increase the signal to noise ratio. The intensity of light emission peaks from each port is first divided by the exposure time and then normalized with the highest intensity peak.

RESULTS AND DISCUSSION

Thermogravimetric Analysis. As shown in Figure 2a, the amorphous boron content of the synthesized BNNTs with the two types of precursors (h-BN and H_3B-NH_3) can be calculated by TGA and the chemical formula for the oxidation reaction of amorphous boron. It was confirmed that the BNNTs synthesized from the h-BN precursor contained 8.88 wt % of amorphous boron, while those synthesized using the H_3B-NH_3 precursor contained 3.16 wt %. The amorphous boron content decreased by approximately three times. In the usual process of TGA for amorphous boron quantification, the temperature increased linearly with a certain rate, and the reaction of amorphous boron with oxygen often did not reach equilibrium owing to the insufficient reaction time at the oxidation temperature. In this study, we increased the temperature at a rate of 5 °C/min, but to obtain more accurate data, we held the temperature for 5 h such that the reaction reached equilibrium at 650 °C. The TGA data showed that there was no mass change after equilibrium.

Raman Spectroscopy and X-ray Diffraction. Although the h-BN and H_3B-NH_3 precursors have similar elemental compositions, their amorphous boron contents differ significantly, indicating that the mechanisms for the two precursors may be different. As shown in the Raman spectroscopic data (Figure 2b), there is no significant difference in the full width at half maximum of the E_{2g} mode of the BNNTs synthesized from the two different precursors.[28] In Figure 2c,d, the XRD data show a clear difference in the peak position of the boron oxide (B_2O_3) contained in the oxidized BNNTs, resulting from the difference in the amorphous boron contents. We sought to compare the boron impurity content in BNNTs synthesized from two different precursors through XRD analysis. However, due to the amorphous structure of boron, it was oxidized to convert it into crystalline boron oxide, which enhanced the signal-to-noise ratio. This method facilitated a distinct demonstration of the disparities in amorphous boron content present in the raw materials. The oxidation process involved heating the BNNTs in an oxygen atmosphere at a rate of 5 °C/min from room temperature to 900 °C. To ensure thorough oxidation, the samples were held at 650 °C for 5 h. In conclusion, it was found that the BNNTs synthesized with AB as a precursor exhibited a lower boron impurity content compared to those synthesized with h-BN as a precursor, leading to a reduced observation of boron oxide.

Comparison of the Number of Walls of the BNNTs. To estimate the number of walls of the BNNTs with different precursors, TEM images containing 130 and 163 BNNTs for the h-BN and H_3B-NH_3 precursors, respectively, were used for identification. As shown in Figure 3c, when H_3B-NH_3 is used as the precursor, the distribution shifts to the left.

For the BNNTs synthesized from the h-BN precursor, the average number of walls was 3.24, with 7.69% single-walled, 41.54% double-walled, 26.15% triple-walled, and 24.62% multiple-walled BNNTs. For the BNNTs synthesized from the H_3B-NH_3 precursor, the average number of walls was 2.44, with 9.20% single-walled, 57.06% double-walled, 22.07% triple-walled, and 11.04% multiple-walled BNNTs. In the case of the H_3B-NH_3 precursor, the average number of walls decreased by 75.3% compared to that of the h-BN precursor,

https://doi.org/10.1021/acsomega.3c00498
ACS Omega 2023, 8, 21514−21521

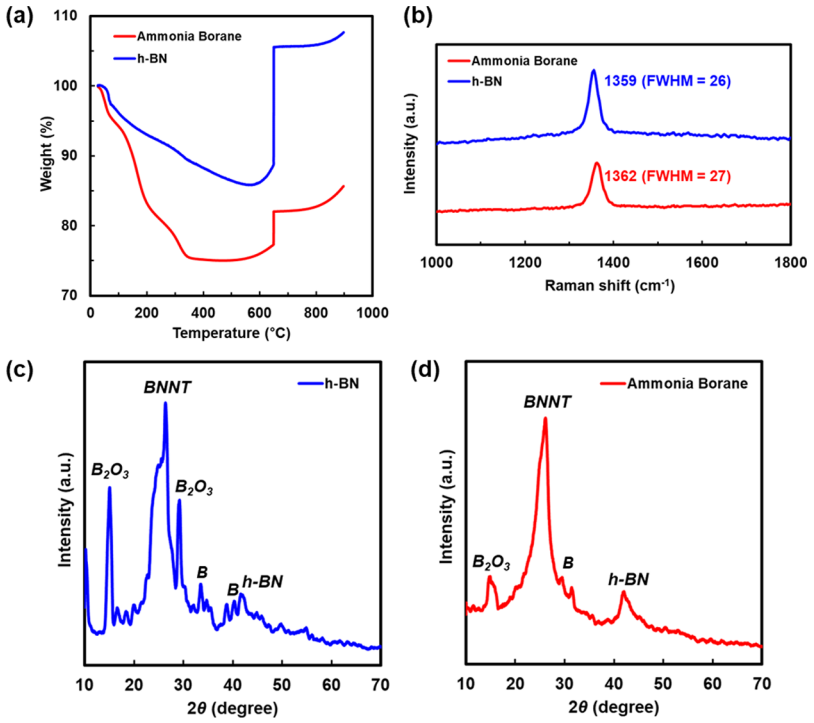

Figure 2. (a) TGA of BNNTs synthesized using h-BN and $H_3B{-}NH_3$. The BNNTs synthesized using h-BN contain 8.88 wt % of amorphous boron, and those synthesized using $H_3B{-}NH_3$ contain 3.16 wt % of amorphous boron; (b) Raman analysis data of BNNTs synthesized from h-BN and $H_3B{-}NH_3$ precursors; XRD analysis data of the oxidated BNNTs synthesized using (c) h-BN and (d) $H_3B{-}NH_3$ precursors.

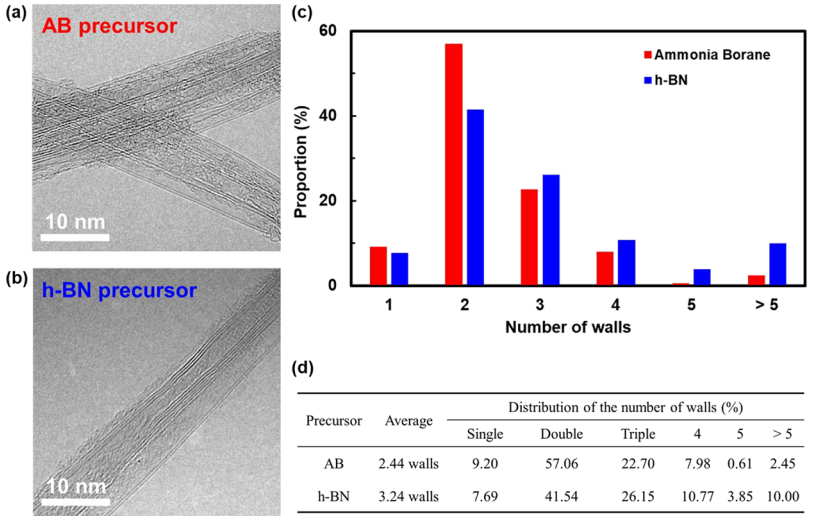

Precursor	Average	Distribution of the number of walls (%)					
		Single	Double	Triple	4	5	> 5
AB	2.44 walls	9.20	57.06	22.70	7.98	0.61	2.45
h-BN	3.24 walls	7.69	41.54	26.15	10.77	3.85	10.00

Figure 3. TEM images of the BNNTs synthesized from (a) AB precursor and (b) h-BN precursor; (c) histogram of the distribution of the number of walls of BNNTs: Red and blue bars correspond to the BNNTs synthesized from the AB precursor and h-BN precursor, respectively; (d) data table of the distribution.

and the proportion of BNNTs with one to three walls increased by 18%.

In Figure 3c, the histograms show the dominant formation of double-walled BNNTs. Unlike CNTs, BNNTs are polarized owing to the difference in the electronegativities between boron and nitrogen, resulting in the formation of a localized electron cloud on the tube surface. Because of the polarities of boron and nitrogen, even though single-walled BNNTs were synthesized during BNNT synthesis at the initial stage, electronegative nitrogen and electropositive boron were attracted to each other via electrostatic forces, possibly forming double-walled BNNTs.

The TEM images (FEI Tecnai at the Core-facility for Bionano Materials in Gachon University) of the BNNTs in Figure 3a,b demonstrate a difference in the number of BNNTs within a bundle, depending on the precursor. An increase in the number of BNNTs within a bundle is observed when $H_3B{-}NH_3$ is used as a precursor than when h-BN is used. The number of BNNTs within a bundle increases proportionally with increasing van der Waals interactions among the BNNTs. The impurities in the synthesized BNNTs reduce the contact area among the BNNTs and weaken the van der Waals forces, preventing the BNNTs from forming bundles. Hence, it is interpreted that the reduction in the impurity content in the

https://doi.org/10.1021/acsomega.3c00498
ACS Omega 2023, 8, 21514−21521

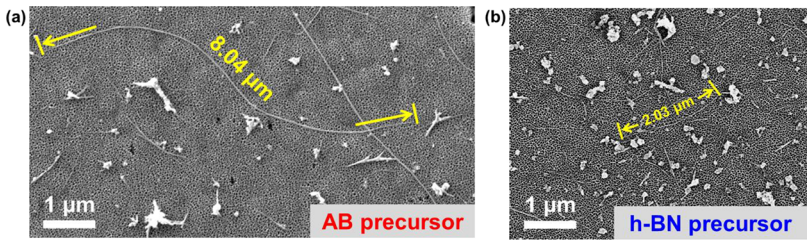

(c)

Number of samples	Average	St. Dev.	Max	Min
100	3.004 μm	1.698 μm	10.366 μm	0.979 μm

(d)

Number of samples	Average	St. Dev.	Max	Min
100	1.323 μm	0.583 μm	3.096 μm	0.340 μm

Figure 4. SEM images of BNNTs synthesized from the (a) $H_3B{-}NH_3$ precursor (b) h-BN precursor. Data table for the lengths of the BNNTs synthesized by the (c) $H_3B{-}NH_3$ precursor and (d) h-BN precursor.

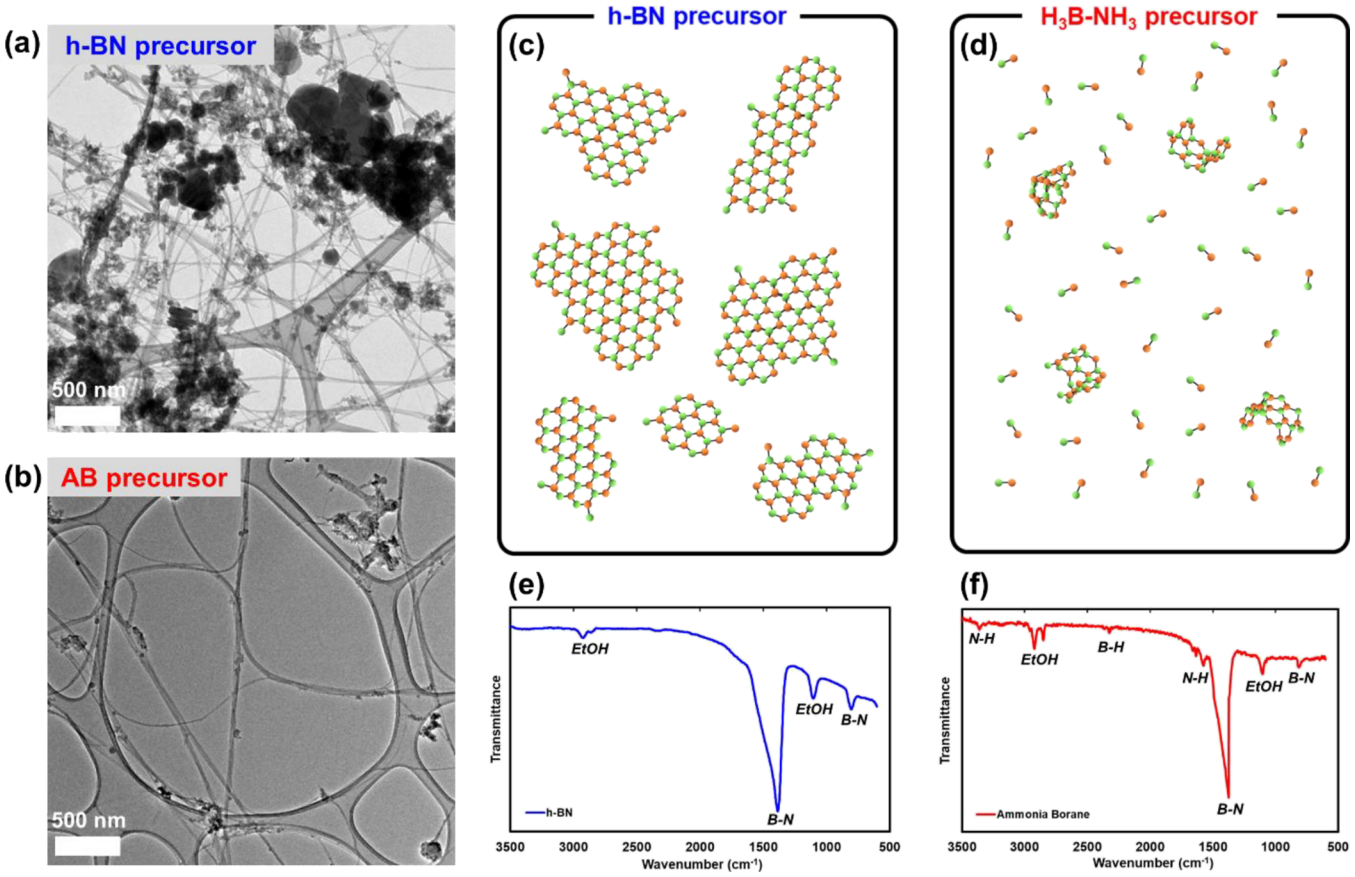

Figure 5. Low-magnitude TEM images of the BNNTs synthesized from the (a) h-BN and (b) $H_3B{-}NH_3$ precursor; imaginary sketch of the decomposed precursor after passing through the RF plasma zone of (c) h-BN and (d) $H_3B{-}NH_3$; FT-IR analysis data of BNNTs synthesized from the (e) h-BN and (f) $H_3B{-}NH_3$ precursor.

BNNTs synthesized from an $H_3B{-}NH_3$ precursor increased the number of BNNTs that form bundles.

Comparison of the Lengths of BNNTs. To confirm the difference in the lengths of BNNTs according to the precursors, 100 BNNTs were analyzed using SEM for h-BN and $H_3B{-}NH_3$. The as-grown BNNTs were obtained in the form of bucky paper. To measure the length of the BNNTs, a process to separate the BNNTs in the bundle was required. The as-grown BNNTs were placed in a certain amount of ethanol and then sonicated for 30 min. Subsequently, the solution was dropped on a Si wafer and observed using SEM. All length data and SEM images of BNNTs using h-BN and $H_3B{-}NH_3$ precursors are shown in Figures S1−S8.

As shown in Figure 4c,d, he BNNTs from the h-BN precursor showed an average length of 1.323 μm, a maximum of 3.096 μm, and a minimum of 0.340 μm, while the BNNTs from the ammonia borane precursor showed an average length of 3.004 μm, a maximum of 10.366 μm, and a minimum of 0.979 μm. In case of the BNNTs with an ammonia borane precursor, the average length was 2.27 times (the maximum length: 3.35 times, the minimum length: 2.88 times) longer than those from the h-BN precursor, implying that the growth rate of BNNTs is much faster.

Comparison of the Amount and Contents of the Impurities. The impurities generated during BNNT synthesis include amorphous boron and h-BN with various structures. The low-magnification TEM images of the synthesized

https://doi.org/10.1021/acsomega.3c00498
ACS Omega 2023, 8, 21514−21521

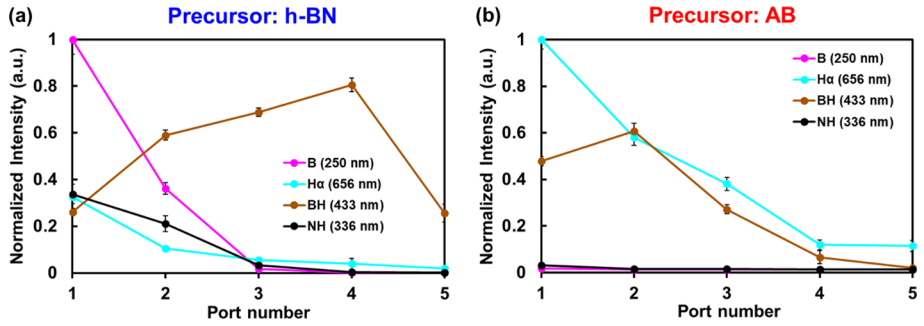

Figure 6. OES analysis of BNNTs synthesized by the (a) h-BN precursor and (b) $H_3B{-}NH_3$ precursor. The meaning of "Port" on the X-axis is as follows: The lower the port number, the closer it is to the energy source and the higher the temperature.

BNNTs in Figure 5a,b show that the contents of amorphous boron and h-BN impurities are considerably lower when using the $H_3B{-}NH_3$ precursor than when using the h-BN precursor.

A difference in the contents of amorphous boron and h-BN impurities was also observed in the FT-IR analysis. According to Harrison et al.,[29] the amount of h-BN impurities can be estimated from the FT-IR peaks of BNNTs and h-BN in the synthesized BNNTs. The out-of-plane versus in-plane transmission (R/TO), which is the ratio of the out-of-plane buckling (R) mode that appears near 800 cm^{-1} and the transverse optical (TO) mode that appears near 1350 cm^{-1}, was used to calculate the h-BN content using the eq R/TO peak ratio = 0.028 + 0.890 × (concentration of h-BN in BNNTs (mg/mg)). In this study, the R/TO ratio of the BNNTs synthesized from the h-BN precursor was 0.4978, and the content of h-BN impurities was calculated to be 52.79 wt %. In contrast, the R/TO ratio of the BNNTs synthesized from the $H_3B{-}NH_3$ precursor was 0.3097, and the content of h-BN impurities was calculated to be 31.65 wt %. These results indicate that the amount of h-BN impurities in the as-grown materials with $H_3B{-}NH_3$ is significantly lower by approximately 1.7 times than that with h-BN.

This difference can be explained based on the mechanism proposed in our previous research,[27] where an $H_3B{-}NH_3$ precursor was used with laser ablation methods. The difference in the amount of h-BN impurities depends on the type of chemical species formed after decomposition, as described in the molecular sketch (Figure 5c,d). For the h-BN precursors, when viewed at the nanoscale, h-BN is fragmented into h-BN planes with lengths of several tens of nanometers, whereas some h-BN precursors are fully decomposed into chemical species such as boron, nitrogen, and BN radicals. As the temperature decreases, the remaining h-BN fragments that do not participate in the BNNT synthesis bond to each other and form a significant amount of h-BN impurities. In contrast, the $H_3B{-}NH_3$ precursor has B−N, N−H, and B−H bonds, and the intramolecular bond strengths are in the order of B−N > N−H > B−H. When energy is applied to $H_3B{-}NH_3$, it dehydrogenates and decomposes into B−N and boron, nitrogen, N−H, and B−H species. BNNTs are formed via the BN self-assembly of these B−N species. When a small number of B−Ns accumulate, they form curvatures to synthesize BNNTs. h-BN impurities are formed when several B−Ns accumulate. We can conclude that the contents of h-BN and amorphous boron impurities depend on the type of precursor used.

In Situ Optical Emission Spectroscopy. In situ OES is measured during synthesis of BNNTs with h-BN and $H_3B{-}NH_3$ precursor thermal plasma. The in situ analysis data for high-temperature thermal plasma synthesis are presented in Figure 6, which show that the mechanism of thermal $H_3B{-}NH_3$ plasma BNNT synthesis is distinct from that of the conventional laser synthesis[19] and thermal plasma synthesis[20] using boron nanoballs. The same is also evident from the results for laser ablation synthesis using $H_3B{-}NH_3$ previously reported by our group.[27]

Port 1 was located at the outlet of the RF plasma zone, which was closest to the energy source, and data were obtained from ports 2, 3, 4, and 5 in that order, away from the plasma zone at the same interval. As plasma discharged in the reactor is blown down from port 1 to port 5, the *x*-axis of the graph (Figure 6) is analogous to the time elapsed from the inlet of the precursor to the end of the process.

The evident difference between the h-BN and $H_3B{-}NH_3$ precursors is that, the existence of boron in the form of boron atomic radical is much more abundant in the synthesis using the h-BN precursor, however it becomes soon under the limit of detection in all the ports when the $H_3B{-}NH_3$ precursor is used for synthesis.

In Figure 6a, when the h-BN precursor is used, high intensity of the boron peak (250 nm) is observed at port 1. At port 2−5, as atomic boron cools down, it condenses into droplet of nano boron to form boron nanoballs, from which the growth of BNNTs can be initiated.[20] Some of the boron atomic radicals react with hydrogen to form BH species, which used for the synthesis of BNNTs.

In Figure 6b, when the $H_3B{-}NH_3$ precursor is used, high intensity of the hydrogen peak (656 nm) is observed at port 1. The abundancy of hydrogen species, which are mostly decomposed from the precursor itself, consumed the atomic boron rapidly to make BH or $B_xN_yH_z$ to inhibit the condensation growth of boron nanoballs. Therefore, the growth of BNNTs needs to start from the self-assembly of the BN themselves, which is similar to that in the laser ablation synthesis of BNNTs with the $H_3B{-}NH_3$ precursor.[27]

CONCLUSIONS

In this paper, we report the synthesis of double-walled BNNTs using $H_3B{-}NH_3$, a molecular precursor, by a high-temperature thermal plasma method. Unlike the conventional method that uses h-BN as a precursor, the content of amorphous boron impurities using this method decreased from 8.88 to 3.16 wt %, and that of h-BN impurities decreased from 52.79 to 31.65 wt %. On comparing the lengths of the BNNTs, those synthesized from the h-BN precursor had an average length of 1.3 μm, while those synthesized from the $H_3B{-}NH_3$ precursor had an

https://doi.org/10.1021/acsomega.3c00498
ACS Omega 2023, 8, 21514−21521

average length of 3.0 μm. The average length increased by 2.3 times when using the H_3B-NH_3 precursor. The average number of walls decreased from 3.24 to 2.44 and double-walled BNNTs dominantly formed by ~60%. Overall, BNNTs with fewer impurities, longer lengths, and fewer walls were synthesized from H_3B-NH_3 compared with those synthesized conventionally using the h-BN precursor, and the production rate significantly increased (~50 g/h). The chemical species formed during the reaction were monitored using in situ OES. Based on these results, the BNNT synthesis in this study was suggested to be based on the self-assembly mechanism of BN radicals, and not the mechanism by which the existing boron nanoballs act as BNNT growth nucleation sites. H_3B-NH_3 formed BN radicals through dehydrogenation on absorbing energy, while the nanosized h-BN formed by combining the BN radicals formed a curvature owing to the excess surface energy and became the nucleus for BNNT growth. This is similar to our previously reported growth mechanism when employing laser ablation with an H_3B-NH_3 precursor. However, it was difficult to identify the reactive species and detailed reactions owing to the limitations of the current research apparatus; this can be considered as a future research direction. Finally, the novel experimental results and data presented in this study will promote the development of BNNTs in academia and the industry.

■ ASSOCIATED CONTENT

Supporting Information

The Supporting Information is available free of charge at https://pubs.acs.org/doi/10.1021/acsomega.3c00498.

Full length data and SEM images of 100 BNNTs synthesized using the ammonia borane precursor and 100 BNNTs synthesized using the h-BN precursor, and certification of the production rate of BNNTs (PDF)

■ AUTHOR INFORMATION

Corresponding Authors

Kun-Hong Lee − *Department of Chemical Engineering, Pohang University of Science and Technology, Pohang, Gyeongbuk 37673, Republic of Korea*; Email: ce20047@postech.ac.kr

Myung Jong Kim − *Department of Chemistry, Gachon University, Seongnam-si, Gyeonggi-do 13120, Republic of Korea*; orcid.org/0000-0002-7484-3081; Email: myungjongkim@gachon.ac.kr

Authors

Dongsu Bae − *Department of Chemical Engineering, Pohang University of Science and Technology, Pohang, Gyeongbuk 37673, Republic of Korea*; orcid.org/0009-0008-1364-3183

Unseok Jung − *Functional Composite Materials Research Center, Korea Institute of Science and Technology, Wanju, Jeollabuk-do 55324, Republic of Korea*

Hunsu Lee − *Functional Composite Materials Research Center, Korea Institute of Science and Technology, Wanju, Jeollabuk-do 55324, Republic of Korea*

Heeil Yoo − *High Enthalpy Plasma Research Center, Jeonbuk National University, Wanju-gun, Jeollabuk-do 565-901, Republic of Korea*

Se Youn Moon − *High Enthalpy Plasma Research Center, Jeonbuk National University, Wanju-gun, Jeollabuk-do 565-901, Republic of Korea; Department of Quantum System Engineering, Jeonbuk National University, Jeonju-si, Jeollabuk-do 54896, Republic of Korea*; orcid.org/0000-0002-6391-3195

Complete contact information is available at: https://pubs.acs.org/10.1021/acsomega.3c00498

Author Contributions

D.B. and U.J. contributed equally to this work. D.B. contributed to characterization of synthesized BNNTs, analysis of experimental data and interpretation of results. U.J. contributed to experiment of BNNT synthesis and in situ OES. H.L. and S.Y.M. contributed to supervise experiment of BNNT synthesis and in situ OES. K.-H.L. contributed to advise manuscript writing and experimental data analysis. M.J.K. contributed to the overall design, direction, and supervision of the project. All authors have given approval to the final version of the manuscript.

Notes

The authors declare no competing financial interest.

■ ACKNOWLEDGMENTS

This work was supported by the grants from the National Research Foundation of Korea (2020R1A2C1101561 and 2021M3F6A1085886) by Korean government (MSIT). This work was also supported by Korea Research Institute for defense Technology planning and advancement (KRIT) grant funded by the Korea government (DAPA (Defense Acquisition Program Administration)) (No. CRIT-CT-21-014, 2021).

■ REFERENCES

(1) Kim, J. H.; Pham, T. V.; Hwang, J. H.; Kim, C. S.; Kim, M. J. Boron nitride nanotubes: synthesis and applications. *Nano convergence* **2018**, *5*, 17.

(2) Arenal, R.; Wang, M.-S.; Xu, Z.; Loiseau, A.; Golberg, D. Young modulus, mechanical and electrical properties of isolated individual and bundled single-walled boron nitride nanotubes. *Nanotechnology* **2011**, *22*, No. 265704.

(3) Suryavanshi, A. P.; Yu, M.-F.; Wen, J.; Tang, C.; Bando, Y. Elastic modulus and resonance behavior of boron nitride nanotubes. *Appl. Phys. Lett.* **2004**, *84*, 2527−2529.

(4) Chopra, N. G.; Zettl, A. Measurement of the elastic modulus of a multi-wall boron nitride nanotube. *Solid State Commun.* **1998**, *105*, 297−300.

(5) Stewart, D. A.; Savic, I.; Mingo, N. First-Principles Calculation of the Isotope Effect on Boron Nitride Nanotube Thermal Conductivity. *Nano Lett.* **2009**, *9*, 81−84.

(6) Dumitrica, T.; Yakobson, B. I. Rate theory of yield in boron nitride nanotubes. *Phys. Rev. B* **2005**, *72*, No. 035418.

(7) Chang, C. W.; Fennimore, A. M.; Afanasiev, A.; Okawa, D.; Ikuno, T.; Garcia, H.; Li, D.; Majumdar, A.; Zettl, A. Isotope Effect on the Thermal Conductivity of Boron Nitride Nanotubes. *Phys. Rev. Lett.* **2006**, *97*, No. 085901.

(8) Chen, Y.; Zou, J.; Campbell, S. J.; Caer, G. L. Boron nitride nanotubes: Pronounced resistance to oxidation. *Appl. Phys. Lett.* **2004**, *84*, 2430−2432.

(9) Weng, Q.; Wang, X.; Wang, X.; Bando, Y.; Golberg, D. Functionalized hexagonal boron nitride nanomaterials: emerging properties and applications. *Chem. Soc. Rev.* **2016**, *45*, 3989−4012.

(10) Blase, X.; Rubio, A.; Louie, S. G.; Cohen, M. L. Stability and Band Gap Constancy of Boron Nitride Nanotubes. *Europhys. Lett.* **1994**, *28*, 335−340.

(11) Lauret, J. S.; Arenal, R.; Ducastelle, F.; Loiseau, A.; Cau, M.; Attal-Tretout, B.; Rosencher, E.; Goux-Capes, L. Optical Transitions

in Single-Wall Boron Nitride Nanotubes. *Phys. Rev. Lett.* **2005**, *94*, No. 037405.
(12) Kang, J. H.; Sauti, G.; Park, C.; Yamakov, V. I.; Wise, K. E.; Lowther, S. E.; Fay, C. C.; Thibeault, S. A.; Bryant, R. G. Multifunctional Electroactive Nanocomposites Based on Piezoelectric Boron Nitride Nanotubes. *ACS Nano* **2015**, *9*, 11942−11950.
(13) Chopra, N. G.; Luyken, R. J.; Cherrey, K.; Crespi, V. H.; Cohen, M. L.; Louie, S. G.; Zettl, A. Boron Nitride Nanotubes. *Science* **1995**, *269*, 966−967.
(14) Golberg, D.; Bando, Y.; Eremets, M.; Takemura, K.; Kurashima, K.; Yusa, H. Nanotubes in boron nitride laser heated at high pressure. *Appl. Phys. Lett.* **1996**, *69*, 2045−2047.
(15) Chen, Y.; Gerald, J. F.; Williams, J. S.; Bulcock, S. Synthesis of boron nitride nanotubes at low temperatures using reactive ball milling. *Chem. Phys. Lett.* **1999**, *299*, 260−264.
(16) Lourie, O. R.; Jones, C. R.; Bartlett, B. M.; Gibbons, P. C.; Ruoff, R. S.; Buhro, W. E. CVD Growth of Boron Nitride Nanotubes. *Chem. Mater.* **2000**, *12*, 1808−1810.
(17) Tang, C.; Bando, Y.; Sato, T.; Kurashima, K. A novel precursor for synthesis of pure boron nitride nanotubes. *Chem. Commun.* **2002**, *12*, 1290−1291.
(18) Zhi, C.; Bando, Y.; Tan, C.; Golberg, D. Effective precursor for high yield synthesis of pure BN nanotubes. *Solid State Commun.* **2005**, *135*, 67−70.
(19) Smith, M. W.; Jordan, K. C.; Park, C.; Kim, J. -W.; Lillehei, P. T.; Crooks, R.; Harrison, J. S. Very long single- and few-walled boron nitride nanotubes via the pressurized vapor/condenser method. *Nanotechnology* **2009**, *20*, No. 505604.
(20) Kim, K. S.; Kingston, C. T.; Hrdina, A. M.; Jakubinek, B.; Guan, J.; Plunkett, M.; Simard, B. Hydrogen-Catalyzed, Pilot-Scale Production of Small-Diameter Boron Nitride Nanotubes and Their Macroscopic Assemblies. *ACS Nano* **2014**, *8*, 6211−6220.
(21) Haber, F. *Fünf Vorträge aus den Jahren 1920−1923*; Verlag von Julius Springer: Berlin, 1924.
(22) Kim, J. H.; Cho, H.; Pham, T. V.; Hwang, J. H.; Ahn, S.; Jang, S. G.; Lee, H.; Park, C.; Kim, C. S.; Kim, M. J. Dual growth mode of boron nitride nanotubes in high temperature pressure laser ablation. *Sci. Rep.* **2019**, *9*, 15674.
(23) Frueh, S.; Kellett, R.; Mallery, C.; Molter, T.; Willis, W. S.; King'ondu, C.; Suib, S. L. Pyrolytic Decomposition of Ammonia Borane to Boron Nitride. *Inorg. Chem.* **2011**, *50*, 783−792.
(24) Zhong, B.; Song, L.; Huang, X. X.; Wen, G. W.; Xia, L. Synthesis of boron nitride nanotubes with SiC nanowire as template. *Mater. Res. Bull.* **2011**, *46*, 1521−1523.
(25) Zhong, B.; Huang, X. X.; Wen, G.; Yu, H.; Zhang, X.; Zhang, T.; Bai, H. Large-Scale Fabrication of Boron Nitride Nanotubes via a Facile Chemical Vapor Reaction Route and Their Cathodoluminescence Properties. *Nanoscale Res. Lett.* **2011**, *6*, 36.
(26) Wang, Y.; Yamamoto, Y.; Kiyono, H.; Shimada, S. Highly Ordered Boron Nitride Nanotube Arrays with Controllable Texture from Ammonia Borane by Template-Aided Vapor-Phase Pyrolysis. *J. Nanomater.* **2008**, *2008*, No. 606283.
(27) Bae, D. S.; Kim, C.; Lee, H.; Khater, O.; Kim, K. S.; Shin, H.; Lee, K.-H.; Kim, M. J. Spontaneous formation of boron nitride nanotube fibers by boron impurity reduction in laser ablation of ammonia borane. *Nano convergence* **2022**, *9*, 20.
(28) Xu, X. G.; Gilburd, L.; Bando, Y.; Golberg, D.; Walker, G. C. Defects and Deformation of Boron Nitride Nanotubes Studied by Joint Nanoscale Mechanical and Infrared Near-Field Microscopy. *J. Phys. Chem. C* **2016**, *120*, 1945−1951.
(29) Harrison, H.; Lamb, J. T.; Nowlin, K. S.; Guenthner, A. J.; Ghiassi, K. B.; Kelkar, A. D.; Alston, J. R. Quantification of hexagonal boron nitride impurities in boron nitride nanotubes via FTIR spectroscopy. *Nanoscale Adv.* **2019**, *1*, 1693−1701.

https://doi.org/10.1021/acsomega.3c00498
ACS Omega 2023, 8, 21514−21521